View Article Online
View Journal

Green Chemistry

Cutting-edge research for a greener sustainable future

Accepted Manuscript

This article can be cited before page numbers have been issued, to do this please use: T. Vu, A. E. E. Alexakis, M. H. Sipponen and M. Andersson, *Green Chem.*, 2026, DOI: 10.1039/D6GC02024K.

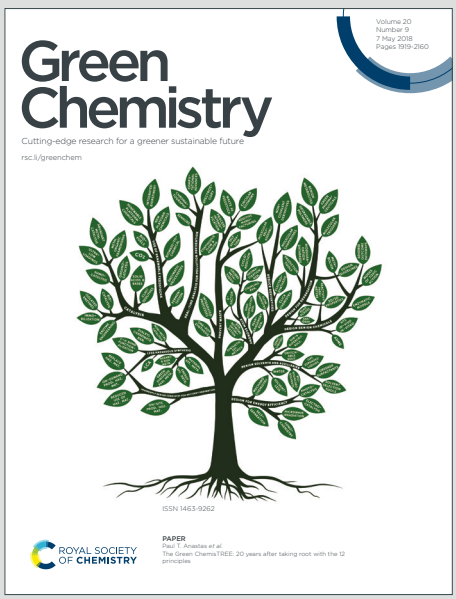

ROYAL SOCIETY OF CHEMISTRY

rsc.li/greenchem

Green foundation

View Article Online
DOI: 10.1039/D6GC02024K

1. This work advances green chemistry in flexible electronic materials by developing a biobased organohydrogel electrolyte. The integration of lignin-derived polymer network with a biobased solvent system reduces reliance on conventional petroleum-derived and toxic dipolar aprotic solvents, providing a safer alternative for organohydrogel design.
2. The materials are synthesized via a catalyst-free method under ambient conditions, minimizing energy input and eliminating hazardous additives. The resulting organohydrogel exhibits good mechanical toughness (10.7 MJ m^{-3}), excellent antifatigue, and high ionic conductivity (4 S m^{-1}) outperforming many previously reported synthetic and lignin-based systems. Sustainability metrics such as E-factor and Process Mass Productivity were employed for quantitative evaluation.
3. Future work may focus on extending this strategy to other renewable polymers toward fully biobased organohydrogels.

View Article Online
DOI: 10.1039/D6GC02024K

ARTICLE

Biobased antifatigue organohydrogel with superior ionic conductivity enabled by lignin nanostructures

Received 00th January 20xx,
Accepted 00th January 20xx

DOI: 10.1039/x0xx00000x

Vu Thanh Truong,[a] Matilda Andersson,[a,b] Alexandros E. Alexakis,[a] and Mika H. Sipponen[a,b*]

Organogels that exhibit efficient mechanical energy dissipation, high mechanical robustness, long-term durability, and outstanding ionic conductivity are promising for flexible electronic devices, yet integrating these attributes into a single material remains an outstanding challenge. Here, we present a hybrid chemically/physically crosslinked biobased double-network organohydrogel synthesized via mild, catalyst-free crosslinking of lignin acetoacetate (LA) in Cyrene-water solvent mixture. The crosslinked LA network serves as the primary reinforcing component, generating a mesoporous structure that simultaneously enables efficient deformation, energy dissipation, and ionic conductivity. This architecture endows the organohydrogel with exceptional mechanical strength, antifatigue under repeated loading, and stable damping capacity at broad temperature and frequency range. As a resistive compression-type sensor, the organohydrogel responds to varying strain levels with consistent and reliable sensitivity. Overall, this family of biobased organohydrogels surpasses fossil-based counterparts and offer strong potential for next-generation flexible electronics.

Introduction

Next-generation flexible ionic conductive devices demand a delicate balance of mechanical properties (high toughness and fatigue resistance), and high ionic conductivity to ensure structural integrity and reliable signal transduction. Optimizing one property often compromises another, making it difficult to achieve all in a single material.[1] Gels are attractive for such applications due to their softness, low weight, and tuneable viscoelasticity,[2] but conventional designs face limitations. Enhancing mechanical robustness through dense physical associations (e.g., hydrogen or ionic bonding, crystalline domains), chemical crosslinks, often compromises ionic conductivity,[3–6] and or reinforcing filler lead to matrix-filer incompatibility, resulting in poor load transfer and inferior damping capacity.[7]

Physically crosslinked networks are prone to irreversible bond rupture and incomplete recovery under cyclic deformation, causing drastic fatigue and hysteresis.[2,8] Hydrogels lose ionic conductivity at subzero temperatures, degrade upon dehydration, and require slow and energy-intensive fabrication, hindering scalability.[5,9,10]

Double-network (DN) gels, composed of a rigid, energy-dissipating network intertwined with a flexible one, overcome the stiffness–toughness trade-off, conferring exceptional strength without brittleness. However, conventional DN gels relying on purely physical entanglements often fail to fully recover after cyclic high-rate or large-impact loading and exhibit pronounced hysteresis, limiting antifatigue and damping performance.[11,12] While highly entangled DN gels with high toughness and low hysteresis have been reported, their combination with high damping capacity and excellent ionic conductivity remains unachieved.[13] Realizing all these properties in a single gel is therefore critical.

Here, we address this challenge by reporting a novel lignin-based hybrid crosslinked double-network organohydrogel that integrates all of these aforementioned attributes. Lignin, an abundant wood-derived macromolecule, was chosen for its inherent rigidity, versatile functional chemistry, and reported ability to promote ionic transport by providing additional interfacial pathways.[9] Using lignin acetoacetate (LA) as the reinforcing and energy-dissipating matrix, we created a biobased, catalyst-free organohydrogel that combines exceptional toughness (10.7 MJ m^{-3}), antifatigue durability, high damping capacity, and ionic conductivity (4 S m^{-1}), outperforming previously reported lignin-based and synthetic gels.

Results and discussion

Synthesis of lignin-based organohydrogels

The hybrid chemically/physically crosslinked lignin-based double-network organohydrogel comprises two complementary networks with distinct functions. The synthesis of the lignin-based organohydrogel is illustrated in Fig. 1a and proceeds via a simple one-pot, catalyst-free method. Soda lignin was first acetoacetylated without catalyst or solvent (Fig. 1a,

[a] Department of Chemistry, Stockholm University, SE-10691, Stockholm, Sweden.
[b] Wallenberg Wood Science Centre, Department of Chemistry, Stockholm University, SE-10691, Stockholm, Sweden.

† Electronic Supplementary Information (ESI) available: Figures S1–S6; Tables S1–S4; References S1–S37. See DOI: 10.1039/x0xx00000x.

View Article Online
DOI: 10.1039/D6GC02024K

ARTICLE

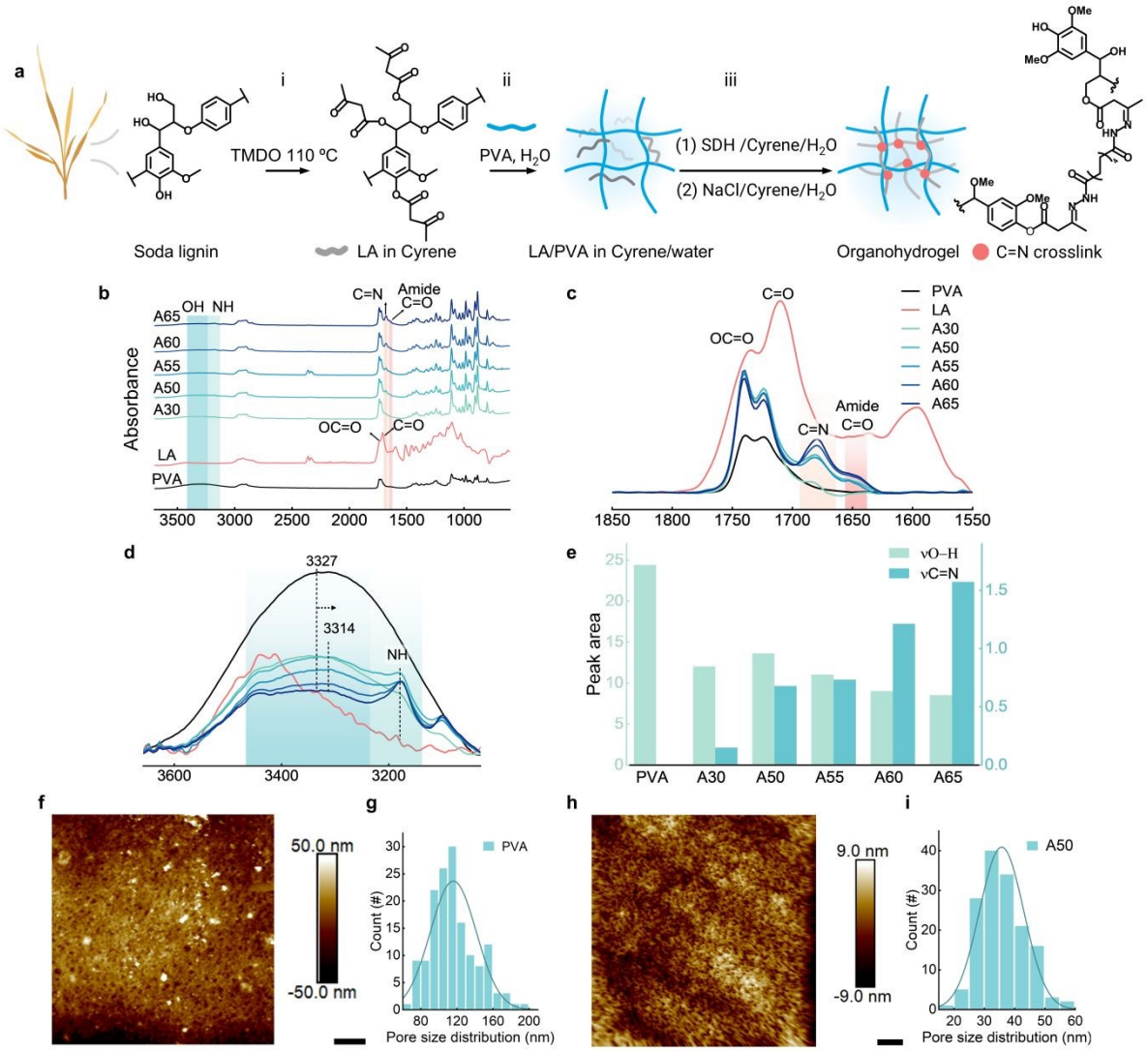

Figure 1. Mesoporous organohydrogel based on LA matrix interpenetrating with PVA. (a) Schematic representation of the synthesis of hybrid crosslinked double-network biobased organohydrogel; (i) acetoacetylation of soda lignin using 2,2,6-trimethyl-4H-1,3-dioxin-4-one (TMDO) and preparation of lignin acetoacetate/Cyrene (LA/Cyrene) solution at varying LA concentration (wt%), (ii) mixing LA/Cyrene solution with aqueous solution of poly(vinyl alcohol) (PVA), and (iii) chemical cross-linking and ions addition by sequential immersion first in sebacic dihydrazide (SDH) and then in sodium chloride 2M (NaCl) solution. (b) FTIR spectra of LA, PVA, and organohydrogel at varying LA contents; (c) Acylhydrazone formation as evidenced in FTIR spectra; (d) Red shift of hydroxyl group shown by FTIR in the ranges of and 3658-3029 cm^{-1}; (e) Quantitative analysis of the peak changes of acylhydrazone and hydroxyl functional groups. (f, h) Atomic force microscopy (AFM) images of pure PVA and A50 (organohydrogel with 50 wt% of LA), respectively, with scale bars of 1 µm (PVA) and 0.5 µm (A50). (g, i) Corresponding pore size distribution for PVA and A50 gels. The Gaussian fitting shows average pore size of 116 ± 25 nm (n = 150) (PVA) and 35 ± 7 (n = 150) (A50).

with the degree of modification shown in Table S1 and Fig. S1. To ensure robust performance under harsh conditions, dihydrolevoglucosenone (Cyrene) was employed as a biobased solvent. LA dissolved in Cyrene was homogeneously mixed with a 20 wt% poly(vinyl alcohol) (PVA) aqueous solution (Fig. 1a, step ii), where its short molecular chains intercalate uniformly with PVA to form a flexible secondary network. Gelation was triggered at room temperature by immersion in sebacic dihydrazide (SDH) in Cyrene solution, where rapid acylhydrazone formation covalently anchors LA within the PVA network (Fig. 1a, step iii).[14] This crosslinking approach generates a dense network of covalent junctions that reinforce the overall matrix. Sodium chloride (NaCl, 2 M relative to the total solvent) was used as the ionic conductor.

Gelation arises from the synergistic effects of formation of crosslinked LA network and solvent-exchange of PVA in the Cyrene/water mixture. In a Cyrene/water mixture (3/2 v/v), Cyrene equilibrates with its geminal diol (Figure 4b, inset), efficiently solvating LA through strong hydrogen bonding, minimizing solvent loss, promoting NaCl ionization for high ionic conductivity, and enhancing PVA crystallinity by competing with water for hydrogen bonding, while the hydrated geminal diol increases polarity and disperses LA uniformly throughout the network.[15] A control experiment with non-functionalized lignin-PVA produced a gel that exhibited phase separation, confirming that covalent crosslinking is essential for forming a uniform matrix (Fig. S2). The formation of acylhydrazone crosslinks was verified by FTIR (Fig. 1b, c). The C=N peak at 1679 cm^{-1} increased in intensity with higher LA content, accompanied by the disappearance of the ketone groups (acetoacetate) of LA at 1710 cm^{-1} (Fig. 1b, c), indicating formation of a crosslinked LA network. Time-dependent FTIR further showed a gradual increase in the C=N intensity, which reached a plateau after approximately 24 h, suggesting the crosslinking reaction approached equilibrium under ambient conditions (Fig. S3). FTIR also provides insight into PVA–LA interactions. Incorporation of LA caused the hydroxyl stretching band to broaden and red-shift from 3325 to 3314 cm^{-1} at 65 wt% LA, along with a decrease in peak intensity by a factor of three, reflecting weakened PVA–PVA hydrogen bonding (Fig. 1d). Fitted peak areas show a decrease in O–H alongside increases in secondary N–H and C=N signals at higher LA content (Fig. 1e), indicating homogeneous LA incorporation and formation of a crosslinked network stabilized by strong hydrogen bonding.[16]

The microstructure was examined by Atomic Force Microscopy (AFM, Fig. 1f and h). In contrast to previously reported lignin-based organogels, which often suffer from lignin aggregation and compromised mechanical performance at 30 wt% lignin content,[9] our organohydrogel contains 50 wt% lignin without aggregation. At this composition, the network exhibits denser, more uniform pore structure with an average pore size of 35 ± 7 nm compared to 116 ± 25 nm for a control PVA organohydrogel. Larger pores in PVA likely arise from excessive polymer swelling during Cyrene–water solvent exchange,[13] whereas the enhanced polarity of Cyrene geminal diol promotes favorable hydrogen bonding among LA, PVA, and solvent, preventing phase separation. These results indicate that the interpenetrating LA network restricts PVA swelling, reduces mesh size, and produces a more uniform porous matrix (Fig. 1f-i).

Network design enables superior mechanical performance

To assess the toughening effect of LA, we performed uniaxial mechanical tests at varying LA contents (wt%) and compared with reference samples of pure PVA and PVA combined with unmodified soda lignin (Fig. 2a, b)**.** The tensile stress-strain curves of all lignin-based organohydrogels exhibited no obvious yielding behaviour, indicating homogenous distribution of stress throughout the network.

Increasing LA content enhanced tensile stress and toughness, reaching a maximum of 3.2 MPa and 10.7 $MJ\ m^{-3}$ at 50 wt% LA (A50), representing 4-time and 9.7-time improvement respectively relative to pure PVA organohydrogel. Beyond 50 wt% LA, mechanical performance decreased, probably due to excessive crosslink density and lignin aggregation, which disrupt homogeneous stress transfer.[17] Nevertheless, at 60 wt% LA the organohydrogel still surpassed the pure PVA organohydrogel in both tensile strength and toughness. Compared to the crosslinked organohydrogels, PVA incorporated with unmodified soda lignin displayed poor dispersion, nonuniform stress concentration, and premature mechanical failure, confirming the role of covalent crosslinking for effective reinforcement (Fig. 2a, b). These results agree with DN gels where high mechanical strength is achieved when one network is highly crosslinked and the other is without crosslinking.[18] Crosslinking density was further adjusted by varying the molar concentration of sebacic dihydrazide (SDH) (Fig. 2c and Table S2). Tensile strength and toughness were optimal with SDH up to 5 mol%, indicating that the acylhydrazone linkage effectively anchored LA within the PVA network and promoted energy dissipation during deformation. The resulting rigid, interpenetrated LA network restricted PVA chain slippage and disentanglement, thereby enhancing load-bearing and fracture resistance. These results are higher than those of synthetic polymer such as poly(dimethyl siloxane) (PDMS) and reported tough gels.[19–21]

The mechanical properties of pure PVA organohydrogel is primarily controlled by the solvent-exchange effect in Cyrene/water solvent mixture, which partially promotes PVA self-association and formation of crystalline domains.[4,15] These crystalline domains suppress fracture propagation but form inhomogeneously, leading to uneven stress concentration and inferior toughness.[4] In contrast, A50 combines solvents-induced crystalline domains with homogeneously distributed LA and uniform crosslink density. Hydrogen bonding between LA acetoacetate groups with PVA hydroxyl group further enhances interfacial compatibility, as evidenced by the red-shift of the stretching OH vibration (Fig. 1d).[22] Subsequent crosslinking yields a continuous, dense network, reflected in the microstructural evolution of PVA upon LA incorporation (Fig. 1f-i). Compared with the PVA organohydrogel, which displays irregular and unevenly distributed pores, A50 exhibits more uniform mesoporous structure that effectively mitigates stress and improves energy dissipation. These synergistic effects provide the confinement necessary for efficient stress relaxation, enabling the simultaneous improvement of strength, toughness, and stretchability.[23,24]

Building on this, we demonstrate that A50 can withstand various mechanical deformations such as stretch, wring, bend, fold, and stab without noticeable mechanical degradation (Fig. 2d). Notably, A50 surpasses previously reported lignin-containing and synthetic gels in tensile strength and modulus. Taken together, these results highlight A50's potential for load-bearing applications, including flexible electronic devices.

View Article Online
DOI: 10.1039/D6GC02024K

ARTICLE

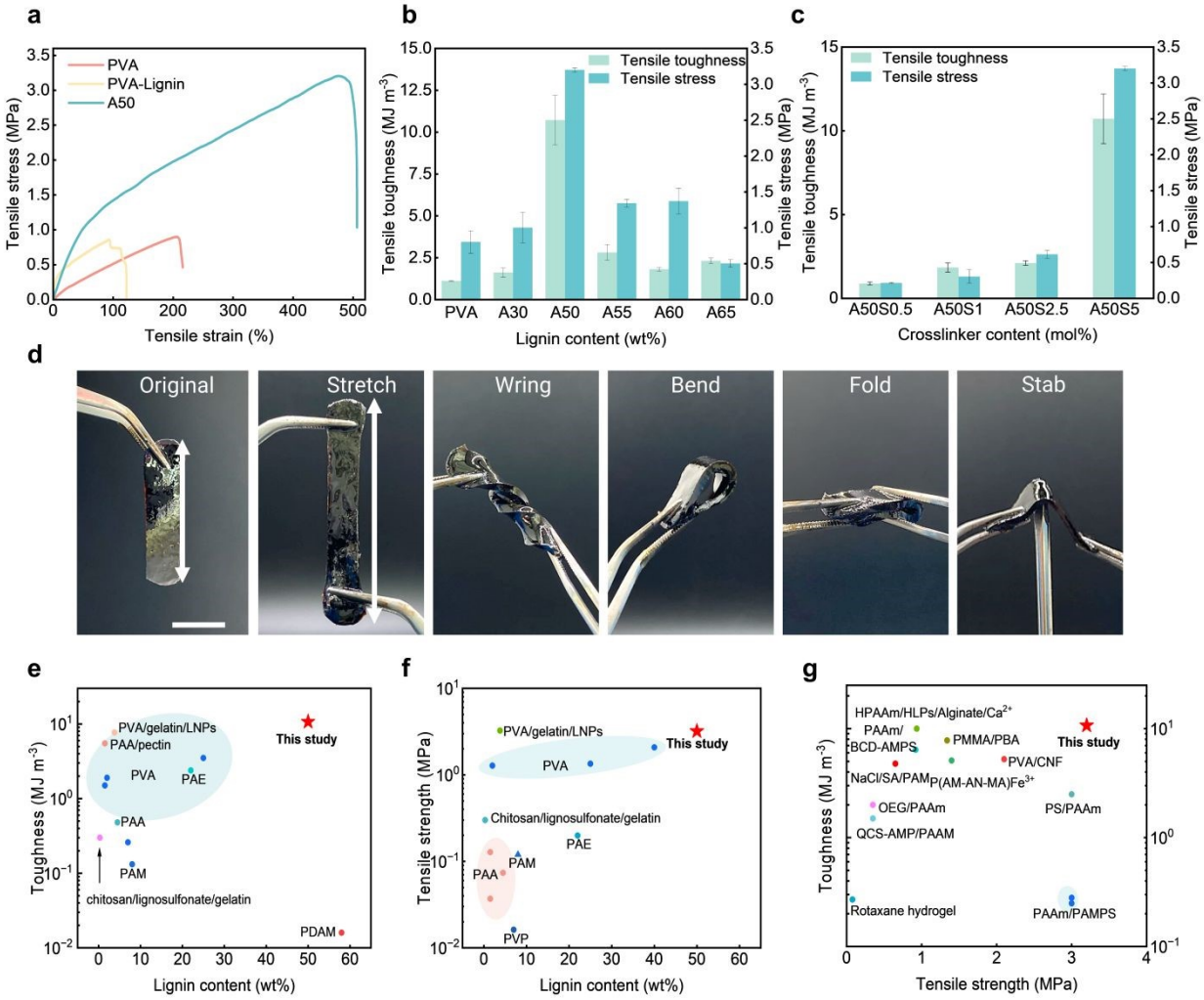

Figure 2 Effect of crosslinked LA matrix and chemical crosslinking density. (a) Mechanical performance of A50 versus pure PVA and PVA-lignin organohydrogel as controls. (b) Tensile toughness and tensile strength of organohydrogel with varying LA contents. (c) Effect of crosslinker (SDH) molar content on tensile toughness and strength where A denotes lignin acetoacetate (LA) weight content (wt%) and S denotes sebacic dihydrazide (SDH) molar content (mol%), respectively. (d) Digital photographs of A50 under different deformations without fracture. (e, f) Ashby plots of fracture toughness and tensile strength as a function of lignin content, comparing A50 with other previously reported lignin-containing gel systems. (g) Ashby plot highlighting the outstanding toughness and tensile strength of A50 versus other synthetic materials.

Stable hysteresis, recovery, and fatigue-resistant performance

Compressive testing revealed the exceptional energy dissipation capacity of A50 organohydrogel. Under compression, it displayed a strength of 3.6 MPa at 80% strain and compression toughness of 0.5 MJ m^{-3}, corresponding to 6.1 times and 5 times those of neat PVA organohydrogel, respectively (Fig. 3a, d). A50 fully recovered from 80% strain without noticeable deformation (Fig. 3a, inset), and its compressive Young's modulus was ~3 times as high as that of the PVA organohydrogel (0.47 versus 0.16 kPa). Unlike single-network gels, which typically face a trade-off between toughness and elastic strength, the hybrid crosslinked lignin-based double-network A50 enhances both. The uniformly distributed nanostructure likely enables the LA-crosslinked network to restrict PVA chain slippage effectively while efficiently dissipating deformation energy.

Hysteresis, the energy loss observed during a loading–unloading cycle, reflects a material's capacity to dissipate energy under repeated deformation, which is critical for maintaining durability and resilience in load-bearing applications. Cyclic compression–relaxation tests of A50

View Article Online
DOI: 10.1039/D6GC02024K

showed pronounced hysteresis, increasing linearly with strain (Fig. 3b, e). At 80% compression, the dissipated energy reached 0.22 MJ m^{-3}, approximately 6.7- and 3.7-times as high as at 50% and 60% strain, respectively, with relative dissipation of ~51%. Minimal hysteresis at 50% strain appears to result from dynamic and reversible events, such as breaking and reformation of sacrificial non-covalent bonds between the PVA and LA networks (e.g., hydrogen bonding, π–π stacking), which facilitate elastic recovery. At higher strains, energy dissipation is dominated by internal friction within the two networks, preventing macroscopic failure. Rate-dependent cyclic tests further supported the presence of two distinct phases of energy dissipation (Fig. 3c, f). At low strain rates (0.5–5 % min^{-1}), energy loss in deformation was governed mainly by the reversible association/dissociation dynamic of physical bonds. At higher strain rates (50–100 % min^{-1}), physical bond could no longer recover within the applied timescale, and the internal friction from the interpenetrating network became dominant. This dissipation behaviour resembles many gel systems such as slide-ring hydrogels which also rely on internal friction.[25]

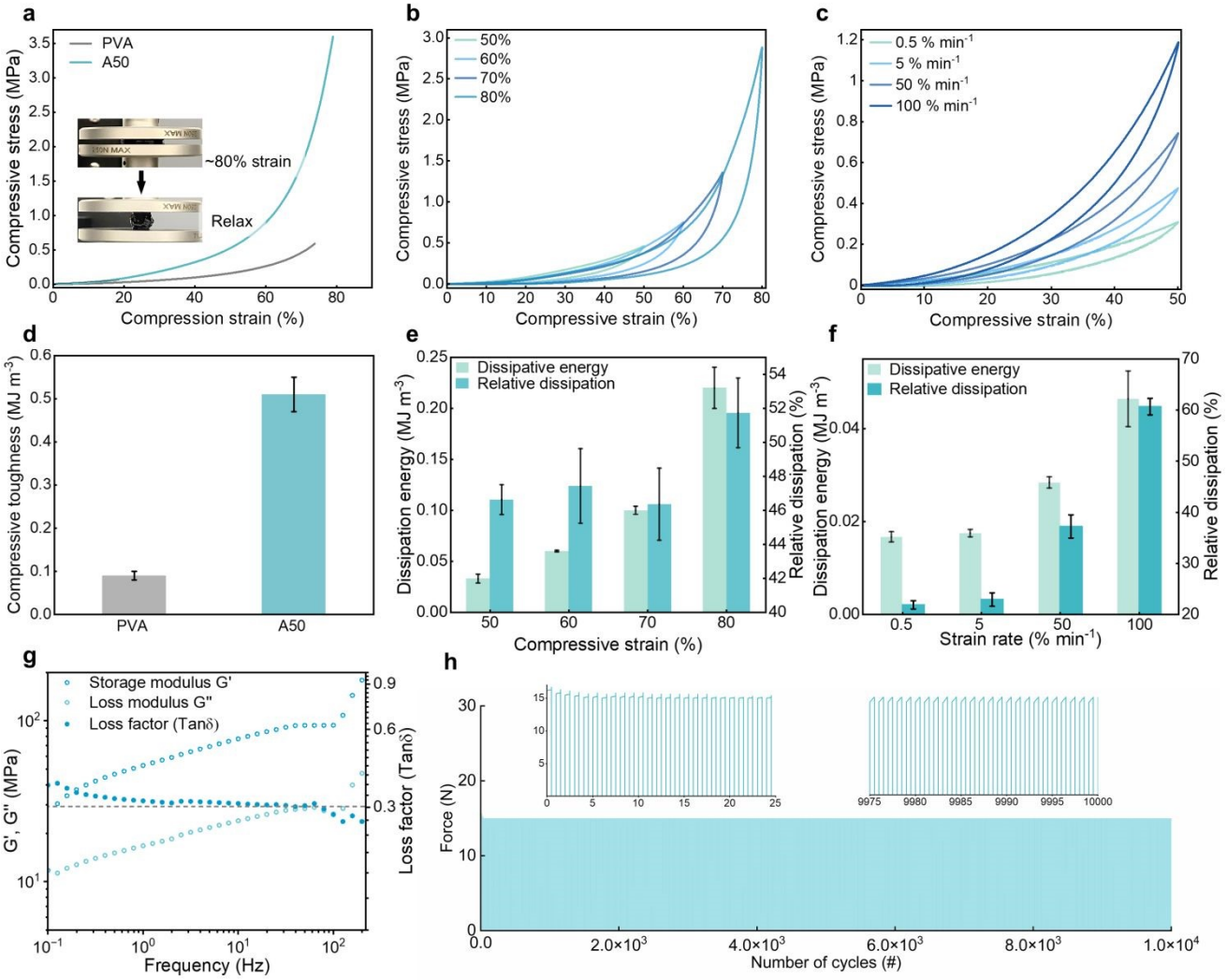

Figure 3. Energy dissipation and anti-fatigue behaviour of hybrid crosslinked lignin-based double network. (a, d) Compression stress–strain curves of A50 and pure PVA (control) and corresponding comparison of compressive toughness. (b, e) Compression-relaxation behaviours of A50 at various strains and corresponding calculated dissipation energy and relative energy dissipation. (c, f) Compressive-relaxation curves at different deformation rates (0.5 % min^{-1}, 5 % min^{-1}, 50 % min^{-1}, and 100 % min^{-1}) at 50% strain with corresponding dissipation energy and relative dissipation. (g) Dynamic mechanical properties of A50 showing decent loss factor (tanδ) over wide range of frequency. (h) Cyclic compression performance illustrating A50 resist 10,000 compression cycles; the inset graphs show the first and last 25 deformation cycles.

The damping performance was further evidenced via the loss tangent tanδ, which is defined by the ratio of loss modulus (G'') to storage modulus (G') in the linear viscoelastic region (Fig. 3g and Fig. S4), reflecting the fraction of mechanical energy dissipated as heat. Deformation energy dissipation arises when the molecular relaxation timescale matches the vibration frequency. The combination of PVA's viscoelasticity and the broad distribution of branched lignin molecules widens the relaxation spectrum, enabling efficient damping across wide frequency range.[26] Importantly, A50 retained its energy dissipation capacity under repeated loading. While a gradual decrease in hysteresis was observed during the first few

View Article Online
DOI: 10.1039/D6GC02034K

hundred compression–relaxation cycles (Fig. S5) the response quickly stabilized, sustaining consistent dissipation and nearly constant compressive strength over 10,000 cycles at 50% strain. Moreover, A50 almost fully recovered after 20 min of rest under ambient conditions following 2000 loading–unloading cycles (Fig. S6). This behaviour suggests initial network rearrangement and partial rupture of sacrificial bonds, followed by stabilization of the crosslinked LA-PVA network. As a result, A50 preserves both damping capacity and mechanical integrity during long-term operation, in contrast to conventional DN gels that typically suffer substantial loss of dissipation due to irreversible fracture of the primary network.[23,27]

Temperature-resilient damping performance

A balanced combination of mechanical strength and damping capacity over a wide temperature range is essential for materials designed to resist impact. Many previously reported damping systems lose elasticity under extreme temperatures or fail to retain their shape due to their highly viscous nature (loss factor > 1).[28,29] In contrast, A50 maintained a nearly constant storage modulus from -50 to 50 °C, and although modulus decreased above 50 °C, the gel remained predominantly elastic (Fig. 4a). A50 also displayed favorable loss factors throughout the examined temperature range (Fig. 4a). Notably, it exhibited a broad damping window, with significant tanδ values from -50 °C to 0 °C, while sustaining high damping capacity (tanδ > 0.3) between 0 °C and 70 °C. Such behaviour rivals benchmark damping elastomers like PDMS and even surpasses conventional damping elastomer.[26,28,30,31]

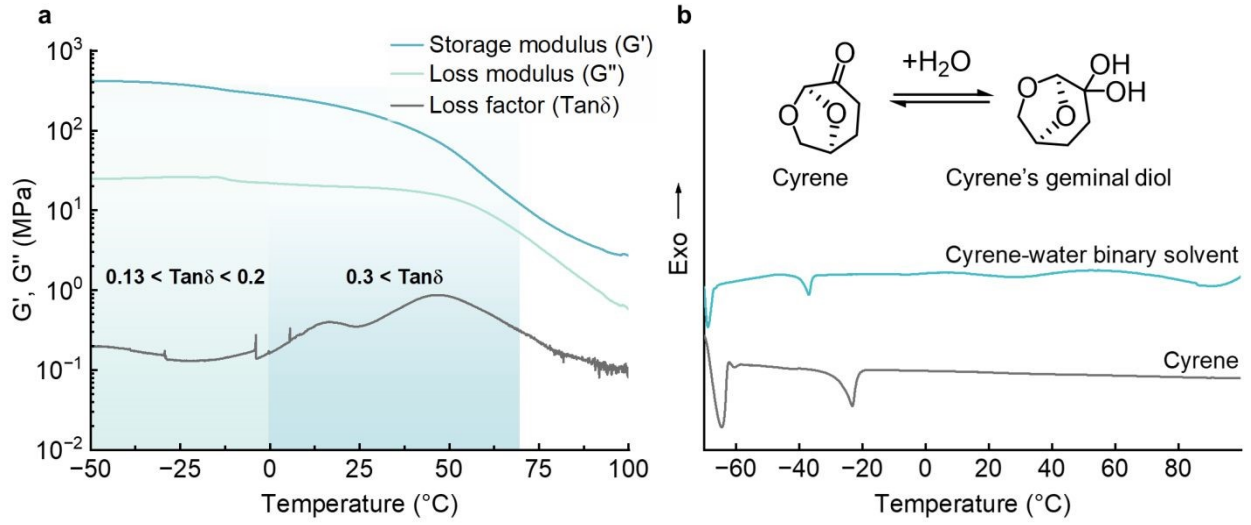

Figure 4. Mechanical and damping performance of organohydrogel at a broad temperature range. (a) Storage (G'), loss modulus (G''), and loss factor (tanδ) of A50 organohydrogel on a temperature ramp from -50 to 100 °C at constant oscillating strain 0.1% at frequency of 1 Hz. (b) Differential scanning calorimetry (DSC) thermogram of Cyrene-water binary solvent and pure Cyrene solvent. The inset scheme illustrates the formation of Cyrene and Cyrene geminal diol in the presence of water.

As discussed, Cyrene's geminal diol act as eutectic solvent and can reduce the freezing point (Fig. 4b).[32] To verify this, we conducted DSC analysis of pure Cyrene and its aqueous mixture at a ratio comparable to that in A50. Pure Cyrene exhibited two exothermic melting peaks at -23 °C and -64 °C, while the Cyrene/water mixture showed peaks at -37 °C and -69 °C. This downward shift in melting temperature supports the formation of Cyrene geminal diol. Moreover, no freezing transition of water was detected, indicating a high fraction of Cyrene and its geminal diol within the mixture. Notably, A50 remained elastic down to -50 °C, which can be attributed to two synergistic effects: (1) the presence of the Cyrene:Cyrene geminal diol:water ternary solvent mixture acting as a deep eutectic system that depresses the freezing point, and (2) freezing point depression arising from solvent confinement within the organohydrogel's mesoporous network.[32,33] The mixture solvent can be considered as deep eutectic solvent that can lower the freezing point. The resulting stability of elasticity across both subzero and elevated temperatures highlights A50's strong potential for applications under extreme environmental conditions.

Ionic conductivity and pressure-sensing performance of the lignin-based organohydrogel

Given its combination of mechanical robustness, damping capacity, and compressibility, A50 was next investigated as a resistivity-type pressure sensor. To impart ionic conductivity, PVA and A50 organohydrogels were immersed in 2 M NaCl/Cyrene/water solution to allow ion diffusion. The Cyrene/water solvent ratio was kept consistent with that of the SDH solution to ensure effective NaCl solvation and to prevent lignin aggregation.

Electrochemical impedance spectroscopy (EIS) revealed pronounced frequency-dependent impedance behaviour (Fig. S7). At low frequencies, A50 displayed high impedance with a negative phase angle, while increasing frequency led to a sharp decrease in impedance and eventual plateau, with the phase angle approaching 0°. This behaviour is characteristic of non-Faradaic ionic conduction, where no charge transfer or migration of electroactive species occurs across the electrode–

electrolyte interface.[4,34] Nyquist plots of both PVA and A50 organohydrogels displayed linear profiles, confirming this interpretation. The bulk resistance, determined from the x-axis intercept of the real impedance (Z'), indicated that A50 possessed twice the ionic conductivity of pristine PVA organohydrogel (Fig. 5a). The enhanced ionic transport at uncompressed state can be attributed to the interconnected mesoporous architecture induced by LA incorporation (Fig. 1h). The reduced pore size increases the specific surface area, creating effective diffusion channels that facilitate efficient ionic transport.[35–38]

Leveraging the rare combination of high mechanical robustness and ionic conductivity, A50 was further employed as a compressive strain sensor, a configuration that requires tolerance to large deformations, strong damping capacity, and reliable signal sensitivity. The device was fabricated by sandwiching an A50 organohydrogel between two copper tape electrodes (Fig. 5c), with a four-wire resistance setup applied to minimize contact resistance effects.

The sensor showed good sensitivity to various extents of strains. As the strain increased from 10% to 50%, the relative resistance change varied systematically from -2.4% to -28.5% over 10 compression cycles, confirming signal precision (Fig. 5b). The organohydrogel sensor maintained a stable signal over 1000 loading-unloading cycles of 50% compressive strain with only minor resistance changes, indicating excellent long-term durability and recoverability (Fig. 5d). After 2000 compression cycles at 50% strain, A50 showed a change in ionic conductivity, i.e., from 4 to 3.98 S/m (Fig. S8) and weight loss of 0.6 wt%, as calculated based on organohydrogel mass before and after cyclic compression. These minimal changes suggest no significant leaching of NaCl or Cyrene/H_2O solvent mixture was observed during the cyclic compression test.

At 50% strain, a gauge factor of 0.6 was obtained, highlighting consistent sensitivity under large deformation (Fig. 5e). The pressure calibration curve exhibits two sensitivity regions with sensitivity (S) of 0.11 kPa^{-1} at pressure below 100 kPa and 0.06 kPa^{-1} above 100 kPa. The high coefficient of determination (R^2) for both regions indicates good linearity and reliable signal accuracy (Fig. S9). This stable response suggests that cyclic compression does not cause significant degradation of the ion-conduction pathways or sensing performance.

Furthermore, owing to its elastic recovery and absence of mechanical degradation under dynamic loading, A50 enabled strain detection across a wide frequency range. The sensor delivered distinct, frequency-dependent resistance patterns (Fig. 5f), remaining stable under both slow compressive loading and rapid impact events. This robust frequency response underscores A50's versatility for real-time monitoring of dynamic mechanical deformations.

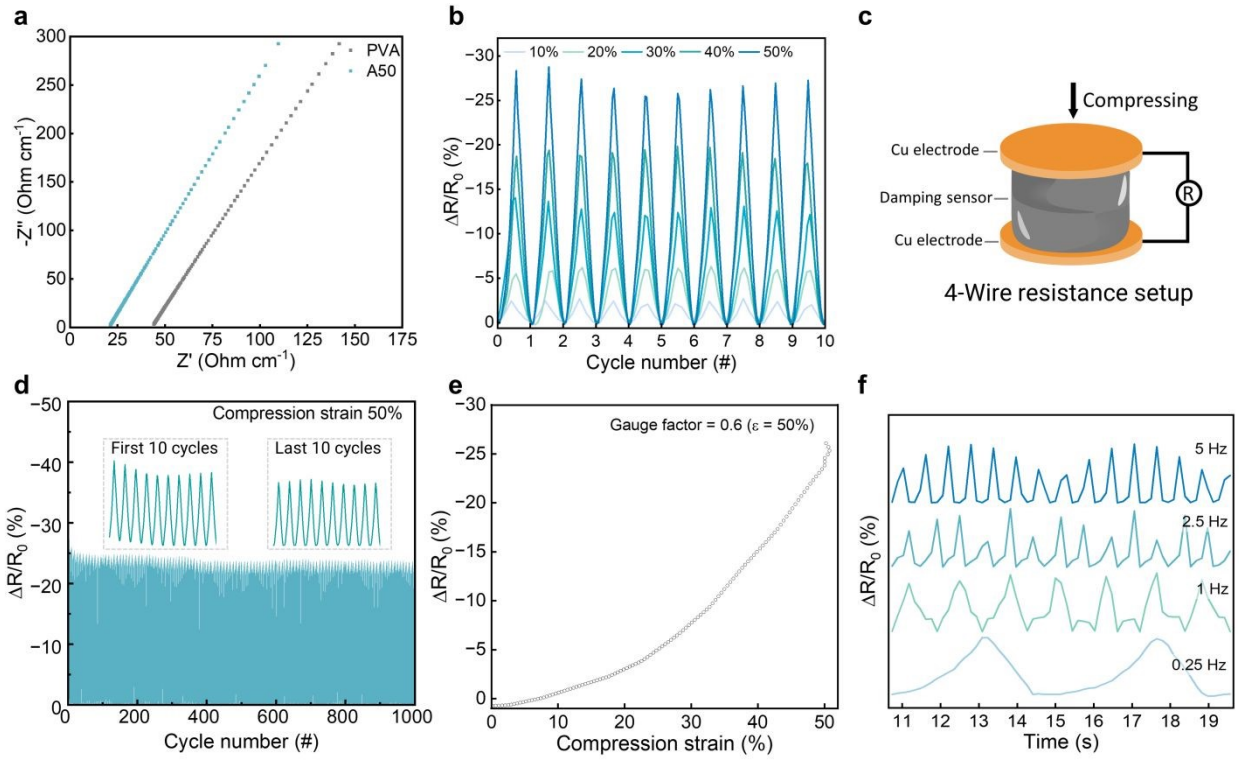

Figure 5. Ionic conductivity and sensing application. (a) Nyquist plots of PVA and A50 showing high conductivity of A50 (4 S m^{-1}). (b) Sensing response at 10%, 20%, 30%, 40%, and 50% compression strain for 10 cycles. (c) Experiment setup monitoring the compressive resistance change. (d) 1000 cycles of the sensing response at 50% compression strain, the insets show the detail of the first and last 10 cycles. (e) Decent compression sensitivity as shown by the gauge factor of 0.6 at 50% strain. (f) Sensing response from compression strain with frequency from 0.25 to 5 Hz.

View Article Online
DOI: 10.1039/D6GC02024K

ARTICLE

Apart from the use of lignin as a renewable feedstock, the present synthesis offers several advantages over previously reported hydrogel and organogel systems. The material is prepared using a safer organic solvent, non-toxic reagents, and a catalyst-free synthesis route, while avoiding energy-intensive steps such as cryogenic drying or freeze-drying that are commonly employed in porous hydrogel synthesis (Fig. 2e–g and Table S3–4). Moreover, the process exhibits an excellent material efficiency and minimal waste generation with an environmental factor (E-factor) of 0.27 and process mass intensity (PMI) of 1.27, which can be further reduced to 0 and 1, respectively when the byproduct can be recovered and reused (Supporting Information). Such quantitative sustainability metrics are rarely reported for hydrogel and organo(hydro)gel syntheses, making benchmarking difficult. In contrast to many reported eco-friendly hydrogel systems that do not fully satisfy key green chemistry principles such as energy efficiency, and waste prevention,[40] this work provides a more rigorous evaluation of sustainability. This system demonstrates a viable strategy for low-waste, sustainable materials synthesis while delivering high performance for flexible electronic applications, offering a versatile platform for the next generation of flexible electronic applications.

Conclusions

We have developed a hybrid chemically/physically crosslinked lignin-based double-network organohydrogel via a simple chemical crosslinking process under ambient conditions. The optimized formulation (50 wt% LA) combines high toughness, compressibility, competitive ionic conductivity, and long-term durability under repeated loading, while maintaining strong damping performance. These properties arise from the lignin-induced mesoporous architecture, which enables efficient energy dissipation and ion transport. At 50 wt% LA, the organohydrogel displayed substantially higher tensile strength and toughness compared to the unmodified lignin control, and its performance exceeded that of both conventional synthetic gels and previously reported lignin-based hydrogels. Incorporation of a biobased liquid phase of aqueous Cyrene imparted the organohydrogel with stable mechanical performance over a wide temperature range (-50 °C to 80 °C). When used as a pressure damping sensor, the organohydrogel delivered reproducible sensitivity and reliable responses across broad strain amplitudes and frequencies. By uniting mechanical robustness, ionic conductivity, thermal tolerance, and sensing capability in a single sustainable material, this work addresses a key challenge in the design of next-generation flexible electronic devices.

Experimental

Materials

Soda lignin (PROTOBIND 2400, GreenValue LLC, purity: 90%) was used to prepare lignin-based organohydrogel in this work. Poly(vinyl alcohol) (average M_w 146000-186000, 87-89% hydrolysed), dihydrolevoglucosenone (Cyrene), sebacic acid dihydrazide (SDH), 2,2,6-trimethyl-4H-1,3-dioxin-4-one (TMDO), isopropanol, sodium chloride (99%), *N*-hydroxy-5-norbornene-2,3-dicarboxylic acid imine, 2-chloro-4,4,5,5-tetramethyl-1,3,2-dioxaphospholane (TMDP), chromium (III) acetyl acetonate, chloroform-d ($CDCl_3$-d_3) were purchased from Sigma-Aldrich. All chemicals were used as received.

Preparation of lignin acetoacetate (LA) and organohydrogels

Preparation of lignin acetoacetate (LA) Soda lignin was acetoacetylated without a catalyst. Briefly, 5g of soda lignin was dissolved in TMDO under a nitrogen environment for 1h to remove moisture. The mixture was then heated to 100 °C and distilled for 3h with nitrogen purging. The product was precipitated with isopropanol, filtered, rinsed with water and dried at 50 °C for further usage and characterization.

Organohydrogel preparation LA was first dissolved in Cyrene at varying concentrations to obtain LA/Cyrene solutions. Meanwhile, PVA aqueous solution (20 wt%) was prepared by continuous stirring for 2 h at 90 °C. The LA/Cyrene solutions were then mixed with PVA aqueous solution, and the resulting mixture was sonicated for 1h to obtain a homogeneous LA/PVA mixture. The total weight of each entry was fixed at 0.4g. The LA/PVA mixture was then transferred to a mold and subsequently soaked in SDH/Cyrene solution (SDH was 5 mol% relative to acetoacetate group content) and allowed to react overnight. To impart ionic conductivity, the resulting organohydrogels, designated as Ax (A refers to LA, x refers to LA weight content wt% (30 - 65 wt%)) were then soaked in NaCl-containing Cyrene/water solution 2M for one day to reach ionic equilibrium. The Cyrene/water volume ratio was kept consistent with that used in the preparation of LA/Cyrene and PVA aqueous solution. For organohydrogels synthesized at different SDH concentrations, the samples were denoted as A50Sy, where y represents the SDH molar content (0.5 – 5 mol%). A control PVA organohydrogel was prepared following the same procedure but immersed in Cyrene without SDH.

Characterization The degree of acetoacetylation was quantified using Phosphorous-31 Nuclear Magnetic Resonance (^{31}P NMR) (400 MHz, Bruker Avance).[39] Briefly, soda lignin and LA were phosphitylated with 2-chloro-4,4,5,5-tetramethyl-1,3,2-dioxaphospholane (TMDP) in the presence of N-hydroxy-5-norbornene-2,3-dicarboxylic acid imine (0.010 mmol), chromium (III) acetyl acetonate, and $CDCl_3$ as internal standard,

relaxation agent, and solvent, respectively. ^{31}P NMR measurements were recorded with following parameters: 128 scans, 5 seconds relaxation delay with 90° pulse and inverse-gated proton decoupling. The organohydrogel surface morphology was examined using a Multimode-8 Atomic Force Microscopy (AFM, Bruker, USA) operated in Peakforce Tapping Mode with ScanAsyst algorithm for self-optimization. ScanAsyst-Air probe was used for all measurements, and the images were then processed using NanoScope Analysis 2.0 software (Bruker, USA). Chemical structure of organohydrogel was confirmed using Fourier Transform Infrared Spectroscopy (Varian 610-IR FTIR spectrometer); spectra were taken in the range of 400–4000 cm^{-1} with a total of 32 scans. Mechanical properties of organohydrogels were measured using Universal Testing Machine (UTM, Instron 5960) equipped with 1 kN load cell. For tensile tests, samples were prepared in a rectangular shape (30 × 5 × 2 mm) and tested at a crosshead speed of 5 mm min^{-1}. Compression stress-strain tests were done on a cylindrical sample (approximately 10 × 10 mm). Compressive/tensile toughness was calculated by integrating the area below the compression/tensile stress-strain until fracture. Dissipation energy was determined using following equation:

$$E = \int_0^{\mathbf{x}} \boldsymbol{\sigma}_{\mathbf{loading}}\mathbf{dx} - \int_0^{\mathbf{x}} \boldsymbol{\sigma}_{\mathbf{unloading}}\mathbf{dx}$$

where $\boldsymbol{\sigma}$ and $\mathbf{x}$ represent compressive stress and strain, respectively. Relative dissipation was determined as:

$$\boldsymbol{\varphi} = \frac{\mathbf{E}}{\mathbf{E_0}} \times \mathbf{100}$$

in which E corresponds to the dissipation energy, and

$$E_0 = \int_{\mathbf{x_0}}^{\mathbf{x}} \boldsymbol{\sigma}(\mathbf{x})\mathbf{dx}$$

with x_0 and x being the starting and maximum compression strain, and $\boldsymbol{\sigma}(\mathbf{x})$ corresponds to the compression curve. For the recovery behaviour test, cyclic loading-unloading at a compression rate of 50 mm min^{-1} was applied without rest. Dynamic mechanical response was analysed using a Dynamic Mechanical Analyzer (Discovery DMA 850). Organohydrogel samples (3.5 mm diameter × 1.5 mm thickness) were first subjected to an oscillation strain sweep (0.01–100%) at room temperature and 1 Hz in tension mode to determine the linear viscoelastic region. Frequency sweep tests were then conducted at 0.5% strain over a frequency range of 0.1–200 Hz. Temperature ramp measurements were carried out from −50 to 100 °C at 1 Hz and 0.1% strain. The ionic conductivity of organohydrogels was measured using the Electrochemical Impedance Spectroscopy (Gamry Interface 1010T, Gamry Instruments Inc) in potentiostatic EIS mode with frequency range from 2×10^4 to 0.1 Hz and 10 mV voltage. Rectangular organohydrogel dimension of 0.2 cm^2 was sandwiched between two stainless steel discs for the measurement. The ionic conductivity was calculated as:

$$\boldsymbol{\sigma} = \frac{\mathbf{L}}{\mathbf{RA}}$$

in which L, R, A are the thickness, impedance value, and contact area of the organohydrogel, respectively. Resistivity-type compressive sensor was designed by sandwiching a cylindrical organohydrogel (dimension 10 × 10 mm) between two copper tapes as electrodes. The resistance was recorded by a digital source meter (Keighley DMM7510), and the resistance change was calculated by

$$\left(\frac{\mathbf{R}-\mathbf{R_0}}{\mathbf{R_0}}\right)\times100\%$$

where R is the dynamic resistance at different strains and R_0 is the initial resistance without strain. Sensitivity is obtained from the slope of relative resistance change ($\Delta R/R_0$) versus pressure.

Author contributions

Vu Thanh Truong: Conceptualization, Formal analysis, Investigation, Methodology, Validation, Visualization, Data curation, Writing – original draft. **Matilda Andersson:** Methodology, Writing – review & editing. **Alexandros E. Alexakis**: Methodology, Writing – review & editing. **Mika H. Sipponen**: Resource, Writing – review & editing, Supervision, Project administration, Funding acquisition.

Conflicts of interest

There are no conflicts to declare.

Acknowledgements

This work was supported by the Swedish Foundation for Strategic Research (SSF, grant FFL21-006) and Swedish Research Council for Sustainable Development (Formas, grant 2021-01952).

Notes and references

1 Li, X. and Gong, J. P., *Nat. Rev. Mater.*, 2024, **9**, 380–398.
2 Hu, L., Chee, P. L., Sugiarto, S., Yu, Y., Shi, C., Yan, R., Yao, Z., Shi, X., Zhi, J., Kai, D., Yu, H.-D. and Huang, W., *Adv. Mater.*, 2023, **35**, 2205326.
3 Xiang, H., Li, X., Wu, B., Sun, S. and Wu, P., *Adv. Mater.*, 2023, **35**, 2209581.
4 Ye, Y., Zhang, Y., Chen, Y., Han, X. and Jiang, F., *Adv. Funct. Mater.*, 2020, **30**, 2003430.
5 Zhang, S., Liu, M., Guo, S., Tieu, A. J. K., Yang, J., Adams, S. and Tan, S. C., *Adv. Funct. Mater.*, 2023, **33**, 2209129.
6 Ding, Y., Zhang, J., Chang, L., Zhang, X., Liu, H. and Jiang, L., *Adv. Mater.*, 2017, **29**, 1704253.
7 Suhr, J., Koratkar, N., Keblinski, P. and Ajayan, P., *Nat. Mater.*, 2005, **4**, 134–137.
8 Wang, S., Yu, L., Wang, S., Zhang, L., Chen, L., Xu, X., Song, Z., Liu, H. and Chen, C., *Nat. Commun.*, 2022, **13**, 3408.
9 Zhang, H., Zhu, Y., Fu, T., Hao, C., Huang, Y., Ren, H., Yan, N. and Zhai, H., *Chem. Eng. J.*, 2024, **485**, 150105.
10 Kuzina, M. A., Kartsev, D. D., Stratonovich, A. V. and Levkin, P. A., *Adv. Funct. Mater.*, 2023, **33**, 2301421.
11 Zhang, M., Yang, Y., Li, M., Shang, Q., Xie, R., Yu, J., Shen, K., Zhang, Y. and Cheng, Y., *Adv. Mater.*, 2023, **35**, 2301551.
12 Lei, H., Dong, L., Li, Y., Zhang, J., Chen, H., Wu, J., Zhang, Y., Fan, Q., Xue, B., Qin, M., Chen, B., Cao, Y. and Wang, W., *Nat. Commun.*, 2020, **11**, 4032.
13 Zhu, R., Zhu, D., Zheng, Z. and Wang, X., *Nat. Commun.*, 2024, **15**, 1344.
14 Kölmel, D. K. and Kool, E. T., *Chem. Rev.*, 2017, **117**, 10358–10376.

View Article Online
DOI: 10.1039/D6GC02024K

15 De Bruyn, M., Budarin, V. L., Misefari, A., Shimizu, S., Fish, H., Cockett, M., Hunt, A. J., Hofstetter, H., Weckhuysen, B. M., Clark, J. H. and Macquarrie, D. J., *ACS Sustainable Chem. Eng.*, 2019, **7**, 7878–7883.
16 Gorman, M., *J. Chem. Educ.*, 1957, **34**, 304.
17 Liu, X., Zhang, H. J., Xi, S., Zhang, Y., Rao, P., You, X. and Qu, S., *Adv. Funct. Mater.*, 2025, **35**, 2413464.
18 Na, Y., Kurokawa, T., Katsuyama, Y., Tsukeshiba, H., Gong, J. P., Osada, Y., Okabe, S., Karino, T. and Shibayama, M., *Macromolecules*, 2004, **37**, 5370–5374.
19 Wu, S., Hua, M., Alsaid, Y., Du, Y., Ma, Y., Zhao, Y., Lo, C., Wang, C., Wu, D., Yao, B., Strzalka, J., Zhou, H., Zhu, X. and He, X., *Adv. Mater.*, 2021, **33**, 2007829.
20 Qu, G., Li, Y., Yu, Y., Huang, Y., Zhang, W., Zhang, H., Liu, Z. and Kong, T., *Angew. Chem., Int. Ed.*, 2019, **58**, 10951–10955.
21 Hu, X., Vatankhah-Varnoosfaderani, M., Zhou, J., Li, Q. and Sheiko, S. S., *Adv. Mater.*, 2015, **27**, 6899–6905.
22 Hao, L. T., Eom, Y., Tran, T. H., Koo, J. M., Jegal, J., Hwang, S. Y., Oh, D. X. and Park, J., *Nanoscale*, 2020, **12**, 2393–2405.
23 Hua, M., Wu, S., Ma, Y., Zhao, Y., Chen, Z., Frenkel, I., Strzalka, J., Zhou, H., Zhu, X. and He, X., *Nature*, 2021, **590**, 594–599.
24 Tolentino, M. A. K., Du, E. Y., Silvani, G., Pandzic, E., Kilian, K. A. and Gooding, J. J., *Adv. Healthcare Mater.*, 2025, **14**, 2500658.
25 Xu, Z., Lu, J., Lu, D., Li, Y., Lei, H., Chen, B., Li, W., Xue, B., Cao, Y. and Wang, W., *Nat. Commun.*, 2024, **15**, 4895.
26 Urayama, K., Miki, T., Takigawa, T. and Kohjiya, S., *Chem. Mater.*, 2004, **16**, 173–178.
27 Pan, X., Li, X., Wang, Z., Ni, Y. and Wang, Q., *ACS Nano*, 2024, **18**, 24095–24104.
28 Wang, Y.-J., He, Y., Zheng, S. Y., Xu, Z., Li, J., Zhao, Y., Chen, L. and Liu, W., *Adv. Funct. Mater.*, 2021, **31**, 2104296.
29 Lin, X., Liu, Y., Bai, A., Cai, H., Bai, Y., Jiang, W., Yang, H., Wang, X., Yang, L., Sun, N. and Gao, H., *Nat. Biomed. Eng.*, 2019, **3**, 632–643.
30 Lei, Z. and Wu, P., *Nat. Commun.*, 2019, **10**, 3429.
31 Cheng, J., Fu, S., Ma, S., Zhang, Z., Ma, C. and Zhang, G., *Adv. Mater.*, 2024, **36**, 2411700.
32 Misefari, A., unpublished work.
33 Majda, D., Makowski, W. and Mańko, M., *J. Therm. Anal. Calorim.*, 2012, **109**, 663–669.
34 Lazanas, A. Ch. and Prodromidis, M. I., *ACS Meas. Sci. Au*, 2023, **3**, 162–193.
35 Shi, J.-L., Tang, C., Peng, H.-J., Lin, Z., Cheng, X.-B., Huang, J.-Q., Zhang, W. and Zhang, Q., *Small*, 2015, **11**, 5243–5252.
36 Fan, L.-Z., Hu, Y.-S., Maier, J., Adelhelm, P., Smarsly, B. and Antonietti, M., *Adv. Funct. Mater.*, 2007, **17**, 3083–3087.
37 Wu, Z.-S., Sun, Y., Tan, Y.-Z., Yang, S., Feng, X. and Müllen, K., *J. Am. Chem. Soc.*, 2012, **134**, 19532–19535.
38 Zhou, Y., Wan, C., Yang, Y., Yang, H., Wang, S., Dai, Z., Ji, K., Jiang, H., Chen, X. and Long, Y., *Adv. Funct. Mater.*, 2019, **29**, 1806220.
39 Meng, X., Crestini, C., Ben, H., Hao, N., Pu, Y., Ragauskas, A. J. and Argyropoulos, D. S., *Nat. Protoc.*, 2019, **14**, 2627–2647.
40 Ballarano, A., Trotta, F., Caldera, F., Hoti, G., López-Nicolás, J. M. and Matencio, A., *Sustain. Chem. Pharm.*, 2025, **48**, 102223.

Data for this article, including all source data will be made available upon acceptance of the manuscript at Zenodo at DOI: 10.5281/zenodo.19394907

View Article Online
DOI: 10.1039/D6GC02024K